Available online at www.sciencedirect.com
ScienceDirect
ELSEVIER
International Journal of Rock Mechanics & Mining Sciences 45 (2008) 763–772
International Journal of Rock Mechanics and Mining Sciences
www.elsevier.com/locate/ijrmms

Influence of intermediate principal stress on rock fracturing and strength near excavation boundaries—Insight from numerical modeling

M. Cai*

Geomechanics Research Centre, MIRARCO, Laurentian University, Sudbury, Ont., Canada P3E 2C6

Received 18 April 2007; accepted 23 July 2007
Available online 18 October 2007

Abstract

The influence of the intermediate principal stress on rock fracturing and strength near excavation boundaries is studied using a FEM/DEM combined numerical tool. A loading condition of $\sigma_3 = 0$ and $\sigma_1 \neq 0$, and $\sigma_2 \neq 0$ exists at the tunnel boundary, where σ_1, σ_2, and σ_3, are the maximum, intermediate, and minimum principal stress components, respectively. The numerical study is based on sample loading testing that follows this type of boundary stress condition. It is seen from the simulation results that the generation of tunnel surface parallel fractures and microcracks is attributed to material heterogeneity and the existence of relatively high intermediate principal stress (σ_2), as well as zero to low minimum principal stress (σ_3) confinement. A high intermediate principal stress confines the rock in such a way that microcracks and fractures can only be developed in the direction parallel to σ_1 and σ_2. Stress-induced fracturing and microcracking in this fashion can lead to onion-skin fractures, spalling, and slabbing in shallow ground near the opening and surface parallel microcracks further away from the opening, leading to anisotropic behavior of the rock. Hence, consideration of the effect of the intermediate principal stress on rock behavior should focus on the stress-induced anisotropic strength and deformation behavior of the rocks. It is also found that the intermediate principal stress has limited influence on the peak strength of the rock near the excavation boundary.

Keywords: Intermediate principal stress; Rock fracturing; Rock strength; Tunnel; Numerical model

1. Introduction

In civil tunneling and underground mining, excavation of an opening alters the stress condition, often from a favorable state to an adverse one. When excavation-induced stresses are high enough, fracturing and failure of the rock masses can result.

The stress state in space is defined by three mutually perpendicular principal stress components (σ_1, σ_2, σ_3). Hence, a general failure criterion for rocks or rock masses should consider the influence of all three principal stress components. To facilitate sound underground engineering and a complete understanding of the constitutive behavior of rocks, mechanical rock mechanics testing and numerical modeling under general stress states and along arbitrary stress paths are needed. Uniaxial and triaxial compressive tests are conducted under the condition of $\sigma_2 = \sigma_3 = 0$ and $\sigma_2 = \sigma_3 \neq 0$, respectively. On the boundary of an unsupported excavation, $\sigma_3 = 0$ and $\sigma_1 \neq 0$, $\sigma_2 \neq 0$ and a state of biaxial stress exists. Away from the boundary, the rocks are in a polyaxial stress state where $\sigma_1 \neq \sigma_2 \neq \sigma_3 \neq 0$, but in general, the minimum principal stress σ_3 is small compared to the other two stress components (Fig. 1). As shown in Fig. 1, σ_1 is the maximum principal (tangential) stress, σ_3 is the minimum principal (radial) stress, and σ_2 is the intermediate principal stress and is often equal to the in situ stress along the tunnel axis.

Failure of brittle hard rocks is a gradual process, which involves microcrack initiation, propagation, and coalescence. In underground excavation and borehole drilling, rock fracturing usually starts at the excavation boundary, at locations where the tangential stress is the highest, and gradually propagates to deeper ground. Rock fracturing is often accompanied by the generation of surface parallel

*Tel.: +1 705 675 1151x5092.
E-mail address: mcai@mirarco.org

1365-1609/$ - see front matter © 2007 Elsevier Ltd. All rights reserved.
doi:10.1016/j.ijrmms.2007.07.026

fractures. This type of failure is called spalling failure, and in many cases, densely spaced "onion-skin" fractures or slabs can be formed.

Onion-skin-type fracturing has been observed in hard rock mines and deep civil tunnels. Two examples are presented in Figs. 2 and 3. The fractures are parallel to the excavation surface, and can only be revealed by cross-cuts or boreholes drilled perpendicular to the excavation surface. The spacing of the stress-induced fractures depends on rock stress and strength conditions as well as the material heterogeneity. The surface parallel fractures such as those shown in Fig. 2(a), where the fracture spacing is relatively large, are sometimes mistakenly recognized by some inexperienced geologists as natural joints, thus greatly underestimates the rock mass quality in the virgin state.

The question to ask is how are the onion-skin fractures formed? Is the intermediate principal stress a contributing factor to the formation of the onion-skin fractures? It is believed that the existence of σ_2 alters the rock fracturing process in such a way that cracks initiate and propagate in a preferred direction. For example, Sahouryeh et al. [2] present an experimental and analytical investigation into 3D crack growth under biaxial compression. They show the importance of the existence of σ_2 by comparing the results of 3D biaxial testing and uniaxial compressive testing. The presence of the intermediate principal stress radically changes the mechanism of crack growth, preventing wing wrapping (curling) and allowing the growing wings extend throughout the tested sample, parallel to the two loading directions. Investigation by Sahouryeh et al. [2] assumes the existence of Griffith cracks and uses experimental and analytical techniques while the present

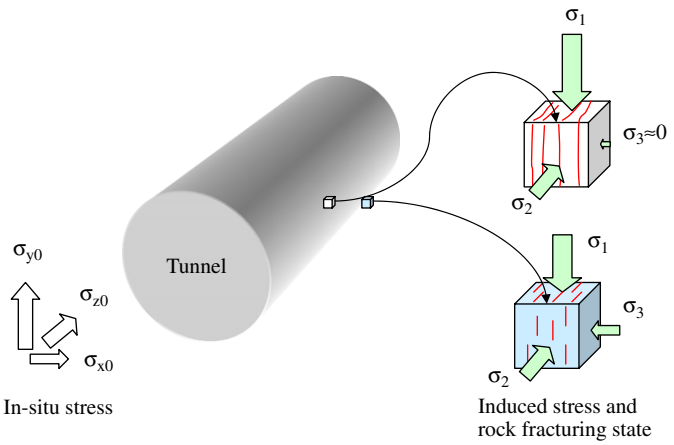

Fig. 1. Stress and rock fracturing condition near the tunnel boundary. σ_{x0}, σ_{y0}, and σ_{z0} are the far-field stress components.

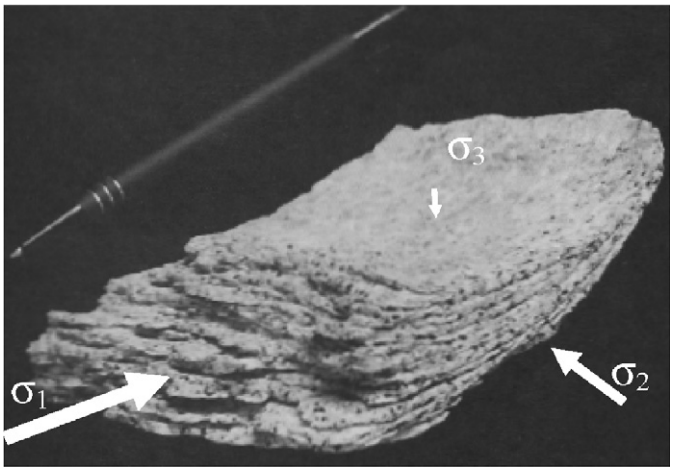

Fig. 3. A granite slab showing the layered fracturing that occurred at the Mine-by tunnel (depth 420 m) at URL [1]. The stress-induced fractures are parallel to the tunnel surface. The orientations of local in situ σ_1, σ_2 (45 MPa), and σ_3 ($\sigma_3 \approx 0$) are illustrated in the figure.

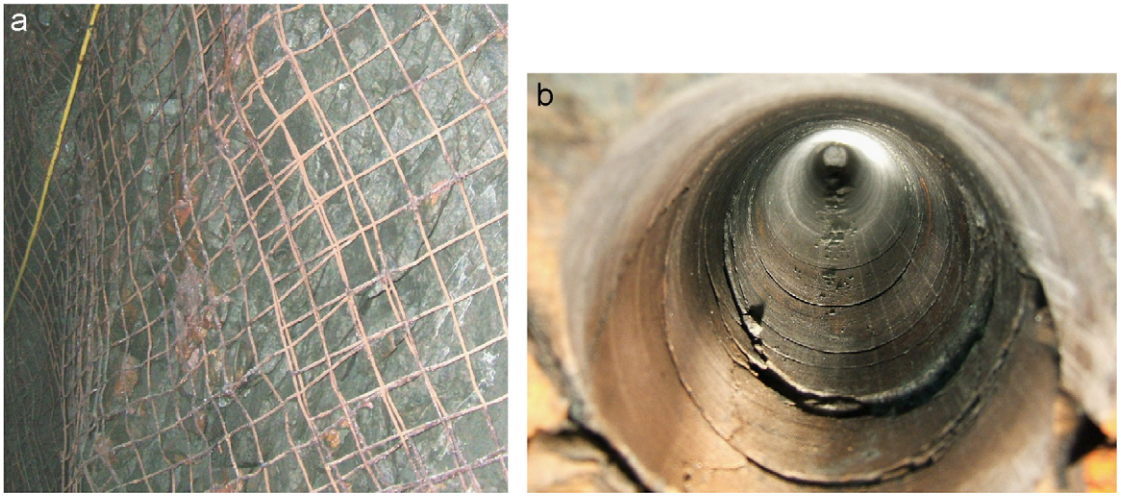

Fig. 2. (a) Surface parallel fractures observed from a cross-cut at Creighton Mine (depth 2500 m) in Canada and (b) surface parallel fractures revealed from a borehole (diameter = 10 cm) in highly stressed ground at Garson Mine in Canada (depth 1500 m; the maximum principal stress is roughly horizontal, and the intermediate principal stress vertical).

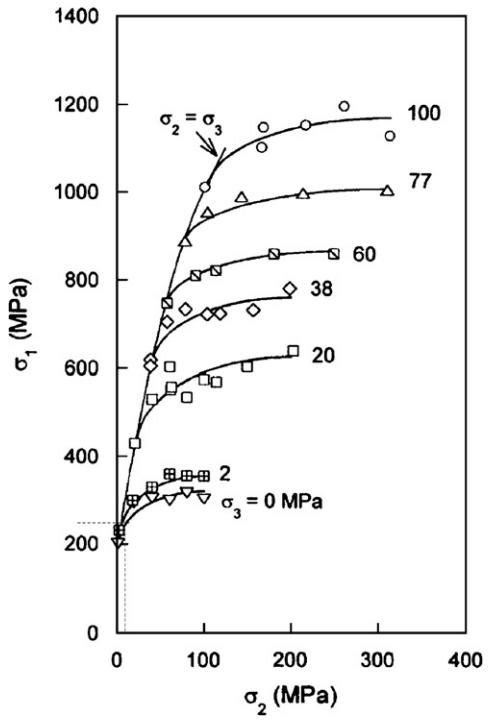

Fig. 4. Influence of the intermediate principal stress on the strength of Westerly granite [7]. Rapid initial rock strength increases with increasing σ_2 can be seen for low σ_3.

paper tries to address questions like these from a different perspective—a numerical simulation approach.

The influence of the intermediate principal stress on rock strength has been studied experimentally [3] and theoretically [4] in the past. Other researchers have developed true triaxial cells to study the behavior of rocks [3,5–7]. Due to end effect, it is difficult to conduct biaxial or true triaxial tests using solid medium loading on cubic or rectangular prisms of rock samples. As pointed out by Brady and Brown [8], the results of polyaxial compression tests are often conflicting, but generally indicate some influence of the intermediate principal stress on stress–strain behavior. One test result on Westerly granite is shown in Fig. 4 [7]. In general, peak strength increases with increasing σ_2 for constant σ_3. Direct observation of the failed sample showed that the specimens developed many micro-cracks and one steeply dipping major fracture that strikes along the direction of applied σ_2 and dips towards σ_3 [7].

Due to access limitation to experimental facilities, true triaxial test results cannot be easily obtained for rocks under consideration in most engineering designs. Hence, the influence of the intermediate principal stress on the most popular failure criteria, such as Mohr–Coulomb and Hoek–Brown failure criteria, is often ignored in engineering practice. Nevertheless, rock failure criteria which consider the influence of σ_2 have been proposed by several researchers [9–13].

To study the rock failure process near an underground excavation, constitutive models describing rock behavior under high σ_1, moderate σ_2, and low σ_3 are required. Variation of test parameters in the stress ranges relevant to underground excavation in the depth range up to 3000 m is needed to explore the sensitivity of the influence of σ_2 on rock strength. Unfortunately, no systematic study results are available from the literature. In addition, direct observation of microcrack developed during true triaxial testing is difficult.

The development of numerical tools in the last thirty years, however, has made it possible to study many of the observed behaviors of rocks in situ. The term "numerical experiment" has been used to describe the practice of using numerical tools to reveal the mechanisms of geomaterials, such as microcrack initiation and propagation, AE (acoustic emission), pressure dependence, non-linear response, volume changes (dilation and compaction), stress-induced anisotropy, transition of stress–strain relation from brittle to ductile, strain softening, difference in compressive and tensile strength, etc. When compared to physical experiments, numerical experiments are quick and can be considered as cost-effective. Parametric studies can also be carried out to reveal the properties that dominate the behavior of rocks.

A FEM/DEM combined numerical tool, which integrates finite element method (FEM) and discrete element method (DEM), is used in the present study to investigate the impact of the intermediate principal stress on rock fracturing and strength near excavation boundaries. Rock heterogeneity is considered in the model, as it is one of the major sources of tensile fracturing in rocks. Heterogeneity of the material data (such as Young's modulus, tensile strength, and fracture energy) is applied at an elemental level, allowing each element to have an independent value assigned for each property. The numerical study strives to simulate the formation of onion-skin fractures observed in deep underground hard rock mines and address the effect of strength enhancement by the intermediate principal stress.

2. Numerical simulation of rock fracturing under polyaxial stress condition

2.1. ELFEN

The finite/discrete element code ELFEN, developed by Rockfield Software Ltd. [14], is used for the numerical simulation in the present study. ELFEN provides a unique ability to model fracture initiation and growth, as well as the extent of damage around excavations under static and dynamic loading conditions. The unique feature of ELFEN is that it simulates the transition of a rock mass from a continuum state to a discontinuous state seamlessly. Creation of new discrete elements and new contact boundaries is performed using fracture and fragmentation algorithms. If the fracture criterion (e.g., Rankine tension, rotating Rankine crack, Mohr–Coulomb with rotating crack) within the intact rock (represented by FEM) is met, then the load carrying capacity across the localized bands

decreases as damage increases until eventually the energy needed to form a discrete fracture is released. At this point, the topology of the mesh is updated, initially leading to fracture propagation within a continuum and eventually resulting in the formation of a discrete element as the rock fragments. Adaptive re-meshing allows the fracture process through the FEM mesh to be tracked and visualized. Most importantly, contact properties (normal and shear stiffness, friction coefficient) can be assigned to pre-existing cracks and newly generated cracks. In subsequent loading, the deformation of these discrete elements is treated rigorously using the DEM algorism and further fracturing of the remaining continuum can be simulated. Recent application of ELFEN to rock fracturing process simulation has demonstrated the effectiveness of the FEM/DEM combined approach [15–20].

In this study, the rock behavior is governed by the rotating Mohr–Coulomb fracture model. This model is able to simulate rock fracturing due to both tension and compression. In tension, the Rankine failure criterion is defined by

$$\sigma_i - \sigma_t = 0, \quad i = 1, 2, 3, \tag{1}$$

where σ_t is the tensile strength. In compression, the Mohr–Coulomb failure criterion is defined by

$$|\tau| = c - \sigma_n \tan\phi = c - \sigma_n \mu, \tag{2}$$

where c is the cohesion strength, ϕ is the internal friction angle, and μ is the coefficient of friction. To model the hardening or softening behavior, the material strength parameters are defined as functions of the effective plastic strain which is defined as

$$\bar{\varepsilon}^p(t) = \int_0^t \sqrt{\tfrac{2}{3}(d\varepsilon_1^p\, d\varepsilon_1^p + d\varepsilon_2^p\, d\varepsilon_2^p + d\varepsilon_3^p\, d\varepsilon_3^p)}\, dt. \tag{3}$$

The functions of the mobilized cohesion and friction angle as well as dilation angle can be established by considering laboratory test data and back analysis of field measurements. In the present study, linearized functions shown in Table 1 are used.

In the rotating Mohr–Coulomb fracture model, it is essentially assumed that in heterogeneous rocks, the fracturing process is an extensional process. Therefore, the failure of a rock in a compressive environment is a result of inelastic extensional strain associated with dilation of rock (Fig. 5). Under a compressive environment, as shown in Fig. 5, the increment of inelastic strain $\Delta\varepsilon_3^p$ in the minimum principal stress direction is extensional. In the model, this increment of extensional strain is associated with tensile strength degradation in the parallel direction, giving

$$\sigma_{t3} = \sigma_{t3}(\varepsilon_3^p) \quad \text{where } \varepsilon_{3n+1}^p = \varepsilon_{3n}^p + \Delta\varepsilon_3^p, \tag{4}$$

where σ_{t3} is the tensile strength in the minimum principal stress direction and n indicates loading step. For the case of linear softening of the tensile strength, one can write

$$\sigma_{t3} = \sigma_{t3}(\varepsilon_3^p) = \sigma_t - H\varepsilon_3^p, \tag{5}$$

Table 1
Material properties used in the simulation

Name	Value			
Young's modulus (GPa)	15 (Variance 30%)			
Poisson's ratio	0.25 (Variance 30%)			
Density ($N s^2/mm^4$)	2.5×10^{-9}			
Tensile strength (MPa)	10 (Variance 50%)			
Fracture energy (J/mm)	0.0001 (Variance 50%)			
Plastic strain	0	0.002	0.004	0.05
Cohesion (MPa)	50	5	5	5
Friction angle (deg)	10	23	40	40
Dilation angle (deg)	0	5	10	10
Contact damping	0.5			
Field (mm)	0.6			
Dem_zone (mm)	3			
Dem_smallest_element (mm)	3			
Normal penalty (N/mm^2)	15 000			
Shear penalty (N/mm^2)	7500			
Friction	0.8			
Contact type	Node-edge			
Factor_critical_time_step	0.7			

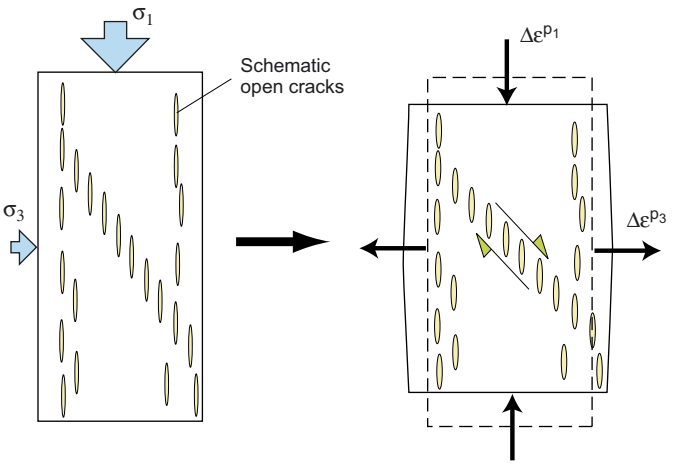

Fig. 5. Extensional strain and failure of rock in compression.

where σ_t is the initial tensile strength and H is the linear softening modulus. For the crack band model in ELFEN, H is given by

$$H = \frac{d\sigma}{d\varepsilon^p} = \frac{h_c^{(e)}}{2G_f}, \tag{6}$$

where $h_c^{(e)}$ is the local element length scale (average dimension) and G_f is the specific fracture energy (fracture energy release rate).

Post initial yielding, the rotating Rankine crack formulation represents the anisotropic damage evolution by degrading the elastic modulus in the direction of the maximum principal stress invariant. The Rankine model uses the same softening model; however, it is applied within

a continuum material formulation rather than by following the direction of cracks or microcracks at a Gauss point.

2.2. Simulation model

Ideally, a 3D tunnel excavation simulation should be conducted to properly consider the excavation process and stress path. However, 3D ELFEN modeling requires extensive computing power, and with current available computer resources, a reasonable model with detailed mesh is not feasible. Hence, as an initial step, a simple prism sample test simulation is conducted. The 3D ELFEN model is presented in Fig. 6(a). The side length of the prism is 50 mm and the height is 100 mm. σ_2 and σ_3 are applied as face loading to the side faces and displacement controlled vertical loading is applied to the sample top surface to generate the maximum principal stress. Three hundred thousand cycling steps are executed, resulting in a total applied displacement of 0.7194 mm at the top of the sample, or 0.72% vertical strain. The bottom of the sample is fixed in the vertical direction. In total, 49 902 unstructured elements are generated as shown in Fig. 6(a). The model parameters are listed in Table 1. Material heterogeneity is considered for the Young's modulus, Poisson's ratio, tensile strength, and fracture energy. This is achieved in ELFEN by assigning the average and variance of a parameter in the input file (.neu). The variances of material heterogeneity are listed in Table 1. Each parameter is varied independently and there is no correlation between tensile strength and Young's modulus. A random number generator is used to create the values for each property on each element. The distribution of the Young's modulus is presented in Fig. 6(b). The scale in the key indicates the ratio of the modulus to the average value. For example, assigning 1.11 for the Young's modulus at a point inside the sample means that the Young's modulus at that point is 11% larger than the average Young's modulus of 15 GPa.

2.3. Results and discussion

2.3.1. Influence of σ_2 on rock fracturing

In tunnel excavation, the minimum principal stress is zero at the boundary and the maximum principal stress, i.e., the tangential stress, is notably magnified as compared to the magnitude of the in situ stress. The intermediate principal stress is often aligned in the tunnel axis direction. As a result, failure is always initiated at the boundary upon excavation and gradually propagates to deep ground away from the opening. The rock fracturing under the stress state of $\sigma_3 = 0$ and $\sigma_1 \neq 0$, $\sigma_2 \neq 0$ is of particular interest to tunnel and borehole stability and is thus investigated in this study.

Fig. 7 presents the fracturing process in uniaxial compression ($\sigma_3 = \sigma_2 = 0$ and $\sigma_1 \neq 0$). Crack initiation is first observed on the sample at a vertical stress level of 48.7 MPa (averaged stress over the sample cross-section). More cracks are generated as the load is increased. The peak strength of the sample is 94.9 MPa, reached when the vertical displacement is 0.6356 mm. More cracks are generated in the post-peak loading stage but in general, the cracks are mostly parallel to the maximum principal

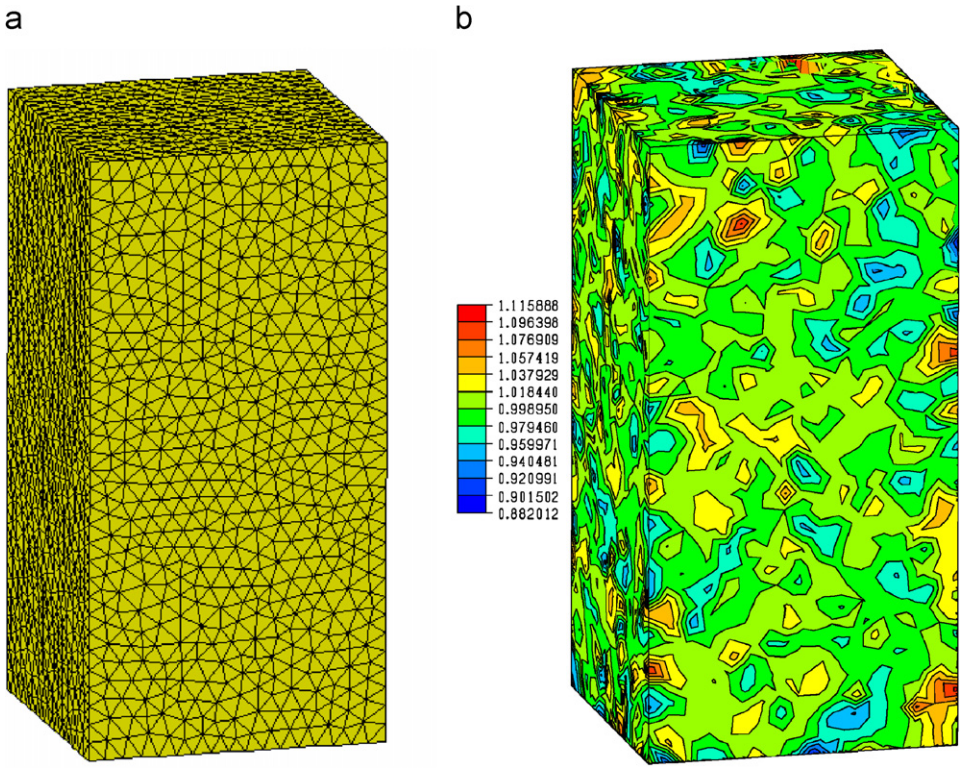

Fig. 6. (a) FEM mesh and (b) distribution of the Young's modulus (the scale in the key indicates the ratio of the modulus to the average value).

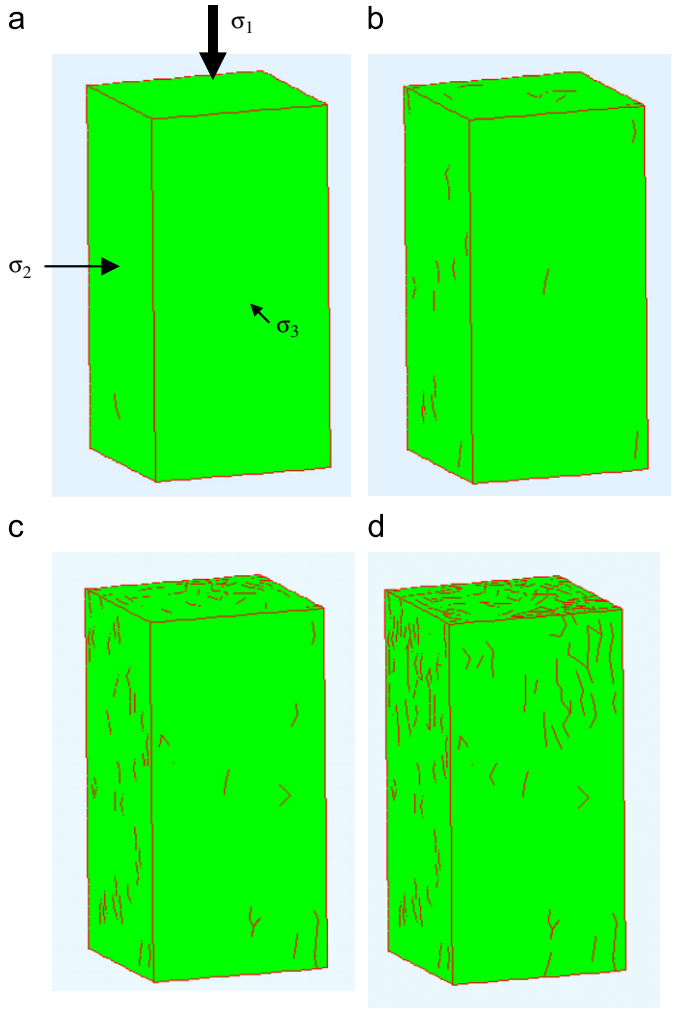

Fig. 7. Rock fracturing process at different σ_1 stress levels ($\sigma_2 = 0$, $\sigma_3 = 0$) for uniaxial loading: (a) 48.7 MPa; (b) 83.2 MPa; (c) 94.9 MPa (peak); and (d) 92.5 MPa (post-peak).

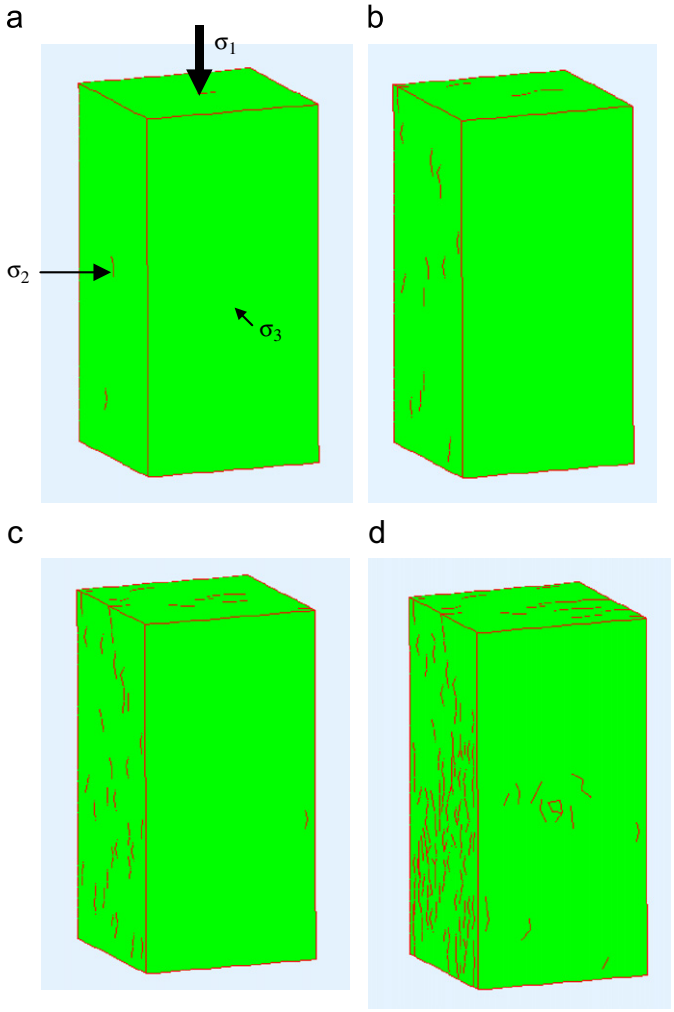

Fig. 8. Rock fracturing process at different σ_1 stress levels ($\sigma_2 = 5$ MPa, $\sigma_3 = 0$): (a) 55.6 MPa; (b) 84.6 MPa; (c) 97.5 MPa (peak); and (d) 91.4 MPa (post-peak).

stress direction and do not have preferred orientations relative to σ_2 or σ_3. The random orientation of the generated fractures can be seen from the top and side of the sample in Fig. 7(d).

The rock fracturing process and the vertical stress–displacement relation are shown in Figs. 8 and 9, respectively, for $\sigma_2 = 5$ MPa and $\sigma_3 = 0$. Since the computation takes very long time to finish, further model running beyond the immediate post-peak strength is not pursued. It is seen from the results that due to the presence of the intermediate principal stress ($\sigma_2 = 5$ MPa), the crack initiation stress level (55.6 MPa) and peak strength (97.5 MPa) are slightly higher than the corresponding values obtained from the uniaxial compression test simulation. Cracks are mostly generated in the orientation parallel to the maximum and intermediate principal stresses. This is because that the existence of the intermediate principal stress suppresses the local tensile stress generated due to material heterogeneity in the rock in a preferred orientation, thus leading to rock fractures formed mostly in the direction parallel to σ_1 and σ_2. As the magnitude of σ_2 further increases to 10 MPa, no fractures will be generated in the orientation perpendicular to the σ_2 direction (Fig. 10). Compared Fig. 10(c) or (d) to the fractures observed near the tunnel boundary (Figs. 2 and 3), it is seen that for the generation of surface parallel fractures or "onion skins," the existence of intermediate principal stress component, in the tunnel axis direction, is a necessary condition. Another necessary condition is the material heterogeneity. Without material heterogeneity, local tensile stress cannot be generated in an overall compressive stress environment so that spalling and slabbing type failure cannot be materialized. In the numerical model, the material heterogeneity is therefore considered. It is observed from the simulation that when $\sigma_2 \geqslant \sigma_t = 10$ MPa, fractures are all oriented parallel to σ_2 because the rock tensile strength is assumed to be 10 MPa and this intermediate principal stress would eventually eliminate all local tensile fractures in the direction perpendicular to σ_2. This is in agreement with what was observed at the Mine-by tunnel at URL in Canada [1]. The stress condition near the tunnel boundary is $\sigma_1 = 169$ MPa, $\sigma_2 = 45$ MPa, and $\sigma_3 \approx 0$ MPa; the tensile strength of the

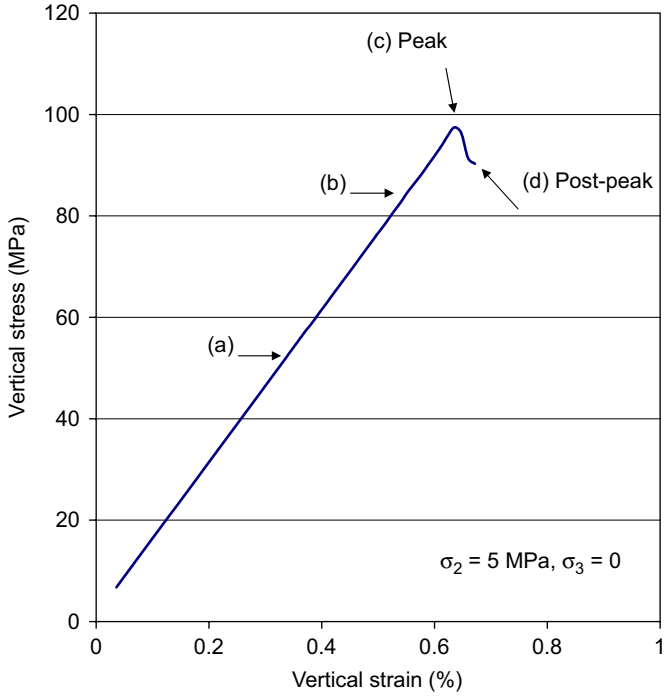

Fig. 9. Vertical stress–displacement relation for $\sigma_2 = 5$ MPa, $\sigma_3 = 0$. The stress levels corresponding to the fracturing states shown in Fig. 8 are indicated in the figure.

rock is estimated to be in the range of 10–15 MPa. Under the given condition, $\sigma_2 > \sigma_t$ holds true so that only surface parallel fractures and microcracks can be generated.

For comparison, the fracture patterns at the end of loading (applied vertical displacement = 0.7194 mm) for different intermediate principal stress levels are shown in Fig. 11. As the intermediate principal stress increases, cracks generated are preferably oriented parallel to σ_1 and σ_2. Brittle failure of rocks and rock masses is associated with the process of crack initiation and propagation, as indicated by AE and volumetric strain monitoring [21,22]. In 3D, the microcracks are planar features. Under uniaxial compression condition or when σ_2 is very small, cracks generated are only parallel to the maximum principal stress σ_1 and have no preferred orientation relative to σ_2 and σ_3 (Fig. 11(a)). Under moderate intermediate principal stress condition, crack initiation in the direction perpendicular to σ_2 is delayed until a higher σ_1 stress level is reached. Cracks are thus mainly formed and propagate in a preferred orientation, i.e., parallel to both σ_1 and σ_2 directions (Fig. 11(b)–(c)). Under a high intermediate principal stress condition, no factures would be observed from the surface on which σ_3 is applied (Fig. 11(d)). In other words, in an underground setting, no fractures would be observed from the tunnel surface under similar condition. This type of rock fracture is difficult to be noticed from the tunnel surface and can only be observed through boreholes (Fig. 3), trenches or cross-cuts, fall-out onion pieces, or indirectly from extensometer monitoring.

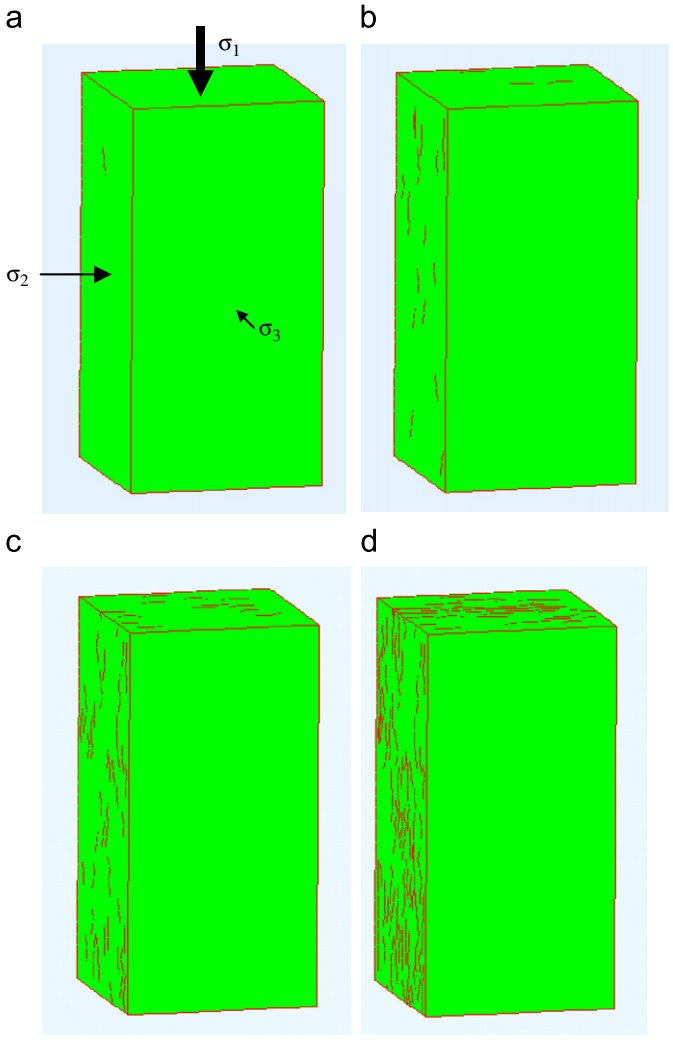

Fig. 10. Rock fracturing process at different σ_1 stress levels ($\sigma_2 = 10$ MPa, $\sigma_3 = 0$): (a) 56.7 MPa; (b) 85.7 MPa; (c) 98.0 MPa (peak); and (d) 89.6 MPa (post-peak).

Colmenares and Zoback [23] noticed that for some rock types (e.g., sandstone and shale), the intermediate principal stress hardly affects failure. This could be because of the fine grain sizes of the rocks that lead to small difference of the microcrack initiation and propagation stress levels and hence limit the influence of σ_2. Rock heterogeneity in sandstone and shale is also small so that spalling and slabbing type failure is difficult to be materialized. Again, field evidence can be found at the URL Mine-by tunnel in Canada that supports this notion. Pronounced notch breakout, resulted from spalling and slabbing, is observed in the coarse grain sized granite whereas in the fine grain sized granodiorite, very little breakout is observed [1].

As fractures in a preferred orientation are generated near the opening, the behavior of the rock becomes anisotropic. This type of anisotropic behavior is stress-induced and the intermediate principal stress plays a major role in the process. Again, field monitoring using micro-velocity probe [24] and micro-seismic monitoring technique, in association

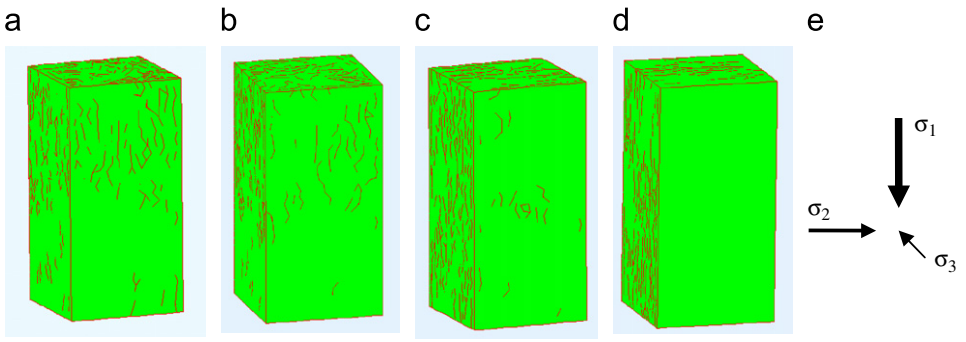

Fig. 11. Rock fracturing patterns at the end of loading (applied vertical displacement = 0.7194 mm) for different intermediate principal stress levels (with $\sigma_3 = 0$): (a) $\sigma_2 = 0$ MPa; (b) $\sigma_2 = 1.5$ MPa; (c) $\sigma_2 = 5$ MPa; and (d) $\sigma_2 = 10$ MPa.

with an anisotropic constitutive model [25], have provided field evidence for the stress-induced anisotropy in the mechanical behavior of rocks. Hence, consideration of the influence of the intermediate principal stress on rock behavior should pay attention to the inclusion of stress-induced anisotropic behavior in the constitutive models.

2.3.2. Influence of σ_2 on rock strength near excavation boundaries

The simulation results indicate that a higher σ_2 delays the onset of crack initiation. In addition, a higher σ_2 increases the peak strength of the rock. All the modeled results show that rock strength, measured by peak σ_1, is higher when a larger intermediate principal stress is applied. The uniaxial compressive strength of the sample is $\sigma_c = 94.9$ MPa. When $\sigma_2 = 10$ MPa, or about 10% of σ_c, the peak strength of the sample reaches 98.0 MPa, an increase of 3.3%. This level of strength increase is obviously smaller than what is observed from the laboratory tests by several researchers [4,5,7]. Based on the strength criterion proposed by Wang and Kemeny [13], the strength will increase at least 18%, 40%, 75% when $\sigma_2/\sigma_c = 0.2$, 0.5, 1.0, respectively. Murrell [26] even suggested a 100% increase of strength when $\sigma_2/\sigma_c = 0.5$ and $\sigma_3 = 0$. A strength increase of about 40–50% can be seen from the test result shown in Fig. 4 when $\sigma_2/\sigma_c = 0.1$ and $\sigma_3 = 0$.

One reason why the laboratory test results show a higher increase of peak strength as the intermediate principal stress increases could be the additional confinement due to the specimen face metal spacers used in the loading system. It is well known that increasing the boundary shear (between the specimen and the loading platen) or decreasing the specimen slenderness (height to width ratio) will yield a high peak stress with a more ductile post-peak stress–strain curve. Although lubricant and copper shim are used [7], the end effect cannot be completely eliminated. In standard UCS and triaxial tests, a sample height to diameter ratio of 2–2.5 is recommended to minimize the end effects. Triaxial tests use oil to apply confinement pressure so that there is no side confinement effect due to loading system. Previous laboratory polyaxial tests employed prism samples with width to height and length to height ratios of 2–2.5. The width to length ratio was 1 in the tests [7]. Obviously, the loading in the σ_2 direction, using stiff platens, will have a "height to diameter" (width to length in the prism sample) ratio (= 1) which is very unfavorable in terms of minimizing the end effect in those laboratory tests [27]. This Poisson's ratio and platen constraint induced end effect can add unwanted confinement in the minimum principal stress direction as the sample deforms. This confinement can increase substantially when microcracks start to develop and the sample dilates, suppressing new crack initiation and propagation of existing cracks, and thus increasing the apparent peak strength of the sample (an increase as large as 50% for low σ_3 confinement is seen from some of the test results (see Fig. 4)).

Other evidence of platen end effect can be seen from the profiles of fractured specimens tested by Haimson and Chong [7]. In their tests, brittle fractures take the final form of a shear band that appears as a steeply inclined fault plane, striking parallel to σ_2 direction and dipping in the σ_3 direction, regardless of the magnitudes of the applied stresses. This is clearly not convincing because spalling type fractures should be observed if σ_3 is very low, as observed in rocks near tunnel boundaries. The fact that spalling failure cannot be identified from test results at $\sigma_3 = 0$ is a clear sign of an end effect that altered the stress condition and hence the failure mode of the test specimen. The formation of shear fractures was never observed in biaxial compression tests conducted by Tayler et al. [28] on concrete samples. In their test, brush bearing platens were used which could minimize the platen end effect. The tested specimens split into thin slabs parallel to the $\sigma_1-\sigma_2$ plane. As summarized in [29], rigid platens may overestimate the material strength by as much as 75%.

In addition, it was noted that in situ rock strength (under condition of $\sigma_2 = 45$ MPa and $\sigma_3 = 0$) back calculated at the URL Mine-by tunnel was not drastically different from the uniaxial compressive strength ($\sigma_c = 213 \pm 20$ MPa) obtained from laboratory tests [1]. If the strength increase inferred from the laboratory polyaxial test result shown in Fig. 4 were true, then, at least a 50% increase of strength under σ_2 confinement ($\sigma_2/\sigma_c = 0.21$) would be expected. This will give an average field strength of about 320 MPa

for the granite at the Mine-by tunnel, which cannot be supported by field evidence. It is seen from the above discussion that end effect does exist in the published polyaxial test results regarding the impact of σ_2 on rock strength.

It is found that the modified Wiebols and Cook polyaxial criterion fits the polyaxial data much better than did the Mohr–Coulomb criterion [23]. Our simulation results agree to the order of strength increase shown by Wiebols and Cook [4], who studied the effect of σ_2 on rock strength theoretically. For $\sigma_3 = 0$ and $\sigma_2/\sigma_c = 0$–10%, the increase in σ_1 is between 0 and 7% (see Fig. 12) according to Wiebols and Cook [4] and the strength increase from this study is about 3.3% under similar condition. Hence, a preliminary conclusion that can be drawn is that the effect of σ_2 on rock strength is small near tunnel boundaries where $\sigma_3 \approx 0$. To further clarify the impact of σ_2 on rock strength, it is suggested to conduct carefully design laboratory tests which minimize the lateral end effect. Innovative design of test facilities, with roller supported loading platen that can follow the lateral deformation of the specimen exactly during the entire test, is required to achieve this goal.

All numerical models and tools have their limitations in representing the true physics of rock fracturing process, and ELFEN is with no exception. Although the "perfect" onion-skin fractures cannot be simulated, the fracture patterns obtained in this study do capture the essential features of the rock fracturing process under a polyaxial stress condition. Field evidence (URL Mine-by tunnel) and theoretical work [4] indicate that the influence of σ_2 on rock strength when $\sigma_3 \approx 0$ is small, and the simulation results of this study tend to agree with this notion. Hence, it is concluded that the numerical tool used for rock fracturing simulation under polyaxial stress condition is robust and realistic. Of course, further improvement of the ELFEN model, including proper consideration of the mesh size, scale-effect, correlation of the material heterogeneity parameters, etc., is required to better simulate the observed rock fracturing process in underground excavations.

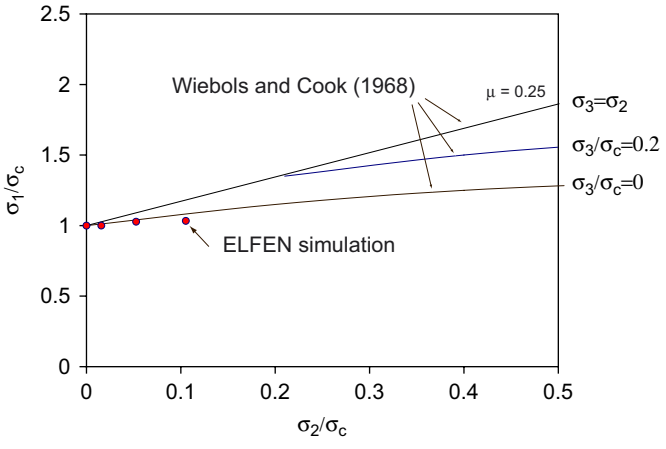

Fig. 12. Comparison of ELFEN simulation results to the theoretical result by Wielols and Cook [4] on the influence of the intermediate principal stress on rock strength.

3. Conclusions

The influence of the intermediate principal stress on rock fracturing and strength is studied using a FEM/DEM combined numerical tool. At the boundary in an underground setting, the intermediate principal stress is often parallel to the tunnel axis, the minimum stress is zero, and the maximum principal stress is the tangential stress. A loading condition of $\sigma_3 = 0$, $\sigma_1 \neq 0$, and $\sigma_2 \neq 0$ thus exists at the boundary. It is seen from the simulation that the generation of tunnel surface parallel fractures (onion skins, spalling and slabbing) is attributed to the existence of moderate intermediate principal stress and low to zero minimum confinement. Material heterogeneity also plays a major role as local tensile stresses need to be generated for crack initiation and propagation. The intermediate principal stress confines the rock in such a way that fractures can only be developed in the direction parallel to σ_1 and σ_2. This fracturing process changes the rock behavior from the original isotropic state to an anisotropic one. Hence, consideration of the effect of the intermediate principal stress on rock behavior should focus on the stress-induced anisotropic strength and deformation behavior of the rocks. Under $\sigma_3 = 0$ condition, it is found that the intermediate principal stress has limited influence on the peak strength of the rock. The large percentage increase of rock strength due to σ_2, as observed from the laboratory tests, is mainly attributed to the end effect of the testing system. Further experimental and numerical study is needed to study the impact of σ_2 on peak strength. In the next phase of the research, it is planed to model the loading platens in ELFEN to quantify the end effect on rock strength.

References

[1] Read RS, Martin CD. Technical summary of AECL's Mine-by experiment, phase 1: excavation response. AECL; 1996. p. 169.
[2] Sahouryeh E, Dyskin AV, Germanovich LN. Crack growth under biaxial compression. Eng Fract Mech 2002;69(18):2187–98.
[3] Mogi K. Flow and fracture of rocks under general triaxial compression. In: Proceedings of the fourth congress ISRM, vol. 3. Rotterdam: Balkema; 1979. p. 123–30.
[4] Wiebols GA, Cook NGW. An energy criterion for the strength of rock in polyaxial compression. Int J Rock Mech Min Sci 1968;5:529–49.
[5] Takahashi M, Koide H. Effect of intermediate principal stress on strength and deformation behavior of sedimentary rocks at the depth shallower than 2000 m. In: Mauri V, Fourmaintraux D, editors. Rock at great depth. Rotterdam: Balkema; 1989. p. 19–26.
[6] Michelis P. A true triaxial cell for low and high-pressure experiments. Int J Rock Mech Min Sci 1985;22:183–8.
[7] Haimson BC, Chang C. A new true triaxial cell for testing mechanical properties of rock, and its use to determine rock strength and deformability of Westerly granite. Int J Rock Mech Min Sci 2000;37(1–2):285–96.

[8] Brady BHG, Brown ET. Rock mechanics for underground mining. London: Chapman & Hall; 1992.
[9] Kim MK, Lade PV. Modelling rock strength in three dimensions. Int J Rock Mech Min Sci 1984;21(1):21–33.
[10] Al-Ajmi AM, Zimmerman RW. Relation between the Mogi and the Coulomb failure criteria. Int J Rock Mech Min Sci 2005;42:431–9.
[11] Desai CS, Salami MR. A constitutive model and associated testing for soft rock. Int J Rock Mech Min Sci 1987;24:299–307.
[12] Pan XD, Hudson JA. A simplified three-dimensional Hoek–Brown yield criterion. In: Romana M, editor. Rock mechanics and power plants, vol. 1. Rotterdam: Balkema; 1988. p. 95–103.
[13] Wang R, Kemeny JM. A new empirical failure criterion for rock under polyaxial compressive stresses. In: Daemen JJK, Schultz RA, editors. Proceedings of the 35th US rock mechanics symposium. Rotterdam: Balkema; 1995. p. 453–8.
[14] Rockfield Software Ltd. ELFEN, Version 3.7, 2003.
[15] Yu JA. Contact interaction framework for numerical simulation of multi-body problems, aspects of damage and fracture for brittle materials. PhD thesis, University of Wales, Swansea; 1999.
[16] Pine RJ, Coggan JS, Flynn ZN, Elmo D. The development of a new numerical modelling approach for naturally fractured rock masses. Rock Mech Rock Eng 2006;39(5):395–419.
[17] Cai M, Kaiser PK. Numerical simulation of the Brazilian test and the tensile strength of anisotropic rocks and rocks with pre-existing cracks. Int J Rock Mech Min Sci 2004;41(Suppl 1):478–83.
[18] Klerck PA. The finite element modelling of discrete fracture of quasi-brittle materials. PhD thesis, University of Wales, Swansea, 2000.
[19] Roberts DP, Sellers EJ, Sevume C. Numerical modelling of fracture zone development and support interaction for a deep level tunnel in a stratified rockmass. In: Hagan TO, editor. SANIRE 99. 1999. p. 264–72.
[20] Eberhardt E, Stead D, Coggan JS. Numerical analysis of initiation and progressive failure in natural rock slopes—the 1991 Randa rockslide. Int J Rock Mech Min Sci 2004;41(1): 69–87.
[21] Martin CD. The effect of cohesion loss and stress path on brittle rock strength. Can Geotech J 1997;34(5):698–725.
[22] Cai M, Kaiser PK, Tasaka Y, Maejima T, Morioka H, Minami M. Generalized crack initiation and crack damage stress thresholds of brittle rock masses near underground excavations. Int J Rock Mech Min Sci 2004;41(5):833–47.
[23] Colmenares LB, Zoback MD. A statistical evaluation of intact rock failure criteria constrained by polyaxial test data for five different rocks. Int J Rock Mech Min Sci 2002;39(6): 695–729.
[24] Maxwell SC, Young RP, Read RS. A micro-velocity tool to assess the excavation damaged zone. Int J Rock Mech Min Sci 1998;35(2): 235–47.
[25] Cai M, Kaiser PK. Assessment of excavation damaged zone using micromechanics model. Tunnell Undergr Space Tech 2005;20(4): 301–10.
[26] Murrell SAF. A criterion for brittle fracture of rocks and concrete under triaxial stress and the effect of pore pressure on the criterion. In: Fairhurst C, editor. Proceedings of the fifth US rock mechanics symposium, 1963. p. 563–77.
[27] Mogi K. Fracture and flow of rocks under high triaxial compression. J Geophys Res 1971;76:1255–69.
[28] Tayler MA, Jain AK, Ramey MR. Path dependent biaxial compressive testing of an all-lightweight aggregate concrete. J Am Concr Inst 1972;69:758–64.
[29] Bobet A. Influence of the loading apparatus on the stresses within biaxial specimens. ASTM Geotech Test J 2001;24(3):256–72.